

Contents lists available at ScienceDirect

# Polymer

journal homepage: www.elsevier.com/locate/polymer



# Prediction-based trade-off analysis of polymer membranes for organic solvent reverse osmosis of hydrocarbons

Young Joo Lee <sup>a</sup>, Janhavi Nistane <sup>b</sup>, Rampi Ramprasad <sup>b</sup>, Ryan P. Lively <sup>a,\*</sup>

- <sup>a</sup> School of Chemical and Biomolecular Engineering, Georgia Institute of Technology, Atlanta, GA, 30332, USA
- <sup>b</sup> School of Materials Science and Engineering, Georgia Institute of Technology, Atlanta, GA, 30332, USA

#### ARTICLE INFO

Keywords:
Organic solvent reverse osmosis
Polymer membrane
Performance trade-off
Solution-diffusion permeation

#### ABSTRACT

Performance trade-off analysis of polymeric membrane materials obtained via experimental studies has been used to select materials for challenging separations and to identify opportunities for innovation. These types of analyses not only highlight the potential and limitations of polymer membranes in different separation applications, but also serve as a reference for guiding the development of new membrane materials and modules. Despite the growing interest in organic solvent reverse osmosis (OSRO) using polymer membranes, a standardized separation performance trade-off curve for OSRO has yet to emerge, primarily due to the limited number of studies in this area. Therefore, there is a need for a comprehensive indicator that reflects the potential separation capabilities of polymer membranes for various organic solvent mixtures. In this study, we generate these performance trade-off curves for >800 polymer structures and three different solvent-solvent separations using a predictive model. Existing data in the literature and new data are used to validate some of the predictions in this work. As OSRO performance is often described in terms of engineering parameters such as permeance and separation factor, we also explore the impact of factors such as permeation resistance in the support layer and the impact of osmotic pressure on separation efficiency.

## 1. Introduction

In nearly all applications of polymer membranes – such as gas separation [1-3], water purification [4,5], and ion separation within electrochemical devices [6] - a trade-off or upper bound exists between productivity (i.e., permeability, the flux normalized by the driving force and the inverse value of membrane thickness) and separation efficiency (selectivity). Typically but not necessarily, polymer membranes that exhibit high permeability tend to have low selectivity between different substances, and vice versa. Consequently, the primary objective of most membrane materials research is to develop membrane materials that can effectively mitigate or overcome this trade-off [7]. In engineering work, these types of trade-off curves are useful in designing membrane technologies and processes, as these often encapsulate the best possible performance achievable via current membrane materials. Of course, these types of trade-off plots are only a small component of the overall membrane construction and operation design, but they are important for process conceptualization and research benchmarking.

These trade-offs or upper bounds have typically been derived from a

database of numerous experimental separation results using polymer membrane materials. As the volume of data increases, the relationship between permeability and selectivity becomes more clearly established, and in some cases, a fundamental justification for the basis of such a trade-off has been developed. Notably, in the field of gas separation membranes, a well-defined relationship has been observed based on the properties of approximately 500-1000 unique polymer membranes for specific gas pairs (O<sub>2</sub>/N<sub>2</sub>, H<sub>2</sub>/N<sub>2</sub>, H<sub>2</sub>/CH<sub>4</sub>, CO<sub>2</sub>/CH<sub>4</sub>, He/N<sub>2</sub>, etc.) [8–10]. A theoretical underpinning developed by Freeman has further solidified this relationship [11–13]. These trade-offs, upper bounds, or distribution of a large set of data points (as a typical trade-off relationship does not always necessarily appear) have become an important reference for many membrane scientists and industry professionals, indicating not only the potential to guide materials development but also the limitations of known polymer membrane chemistries. However, in the relatively nascent field of organic solvent reverse osmosis (OSRO) separations, these types of performance trade-offs remain undeveloped due to a lack of comprehensive data and practical predictive models. We suggest that the development of these performance trade-offs will better

This article is part of a special issue entitled: Polymer Membranes published in Polymer.

E-mail address: ryan.lively@chbe.gatech.edu (R.P. Lively).

<sup>\*</sup> Corresponding author.

enable membrane process conceptualization and identify opportunities for future membrane materials research, and that these trade-offs can be initially generated using predictive models with experimental validation.

Several machine learning (ML) models have been developed based on widely reported data on pure solvent permeation [14-18]. These models can potentially predict the permeability of common organic solvent molecules (i.e., toluene, alkanes, alcohols, ketones etc.) within polymer membranes. However, it is challenging to account for the variety of chemicals used in industry, which are often different from the common solvents. Moreover, there are limitations to the number of polymer chemical structures to which the models can be applied. Although some models are capable of predicting the permeability of any pure solvent within a random polymer membrane, they fail to account for the variations in separation results that arise from compositions of different substances within the polymer membrane when dealing with mixtures. More importantly, it is critical to recognize that inferring ideal permselectivity – defined as the ratio of pure component permeabilities for two different species - whether obtained experimentally or predicted, is of limited engineering relevance for OSRO separation. This is because, in actual separations involving mixtures, competitive sorption, diffusion coupling, and potential changes in polymer chain dynamics induced by plasticization effects from one or multiple solvent species can alter the transport behavior compared to pure component permeation [19-21]. As a result, the separation behavior of mixed organic solvent systems cannot be reliably extrapolated from pure component permeability coefficient data alone.

The primary purpose of this work is to generate the initial set of performance trade-off curves for polymer membrane-based OSRO separations of several classes of hydrocarbon mixtures using a predictive model [21-23]. In this model, the diffusivity and sorption uptake of the pure solvent within the polymer membrane are first predicted using two machine learning (ML) models developed previously (ML diffusion model and ML sorption model). These predicted parameters are then incorporated into a Maxwell-Stefan-based solution-diffusion permeation framework, enabling the final prediction of the polymer membrane's separation performance (e.g., permeance and separation factor) for a given mixture. Note that the separation performance (permeance, separation factor) derived in this work reflects the permeation of an actual binary mixture, not simply the permeability of pure components or an ideal permselectivity obtained under the assumption of zero activity on the downstream side. In this work, three different mixtures - toluene/1, 3,5-triisopropylbenzene, toluene/iso-octane, and n-octane/iso-octane – as representatives of aromatic-aromatic, aromatic-aliphatic, and aliphatic isomer separations are studied. Separation performances for these mixture classes are predicted for a total of 857 polymer membranes that have been widely used in gas and organic solvent separations [23,24]. A subset of these predictions is validated by new experiments discussed in this work as well as previously published experimental data. In addition, it is impractical to use freestanding membranes with a thickness of hundreds of nanometers to 1 µm in laboratory or industrial applications. Instead, an asymmetric membrane that consists of a thin selective layer integrated with, or on a porous and mechanically robust support layer is more practical [25-27]. Considering that this support layer also introduces resistance to the permeation of the mixture through the membrane, a permeation resistance model is envisioned and incorporated in the flux calculations. Lastly, this work also examines the changes in the landscape of polymer membrane-based OSRO at varying feed mixture concentrations.

#### 2. Materials and methods

#### 2.1. Materials

In this work, three polymer materials (Matrimid, SBAD-1, and DUCKY-9 in Fig. S1) were fabricated as thin film composite membranes

and tested for two types of binary hydrocarbon mixtures (e.g., toluene/iso-octane, n-octane/iso-octane) used as a small set for experimental validation. The prediction validation for toluene/TIPB separation was conducted on previously reported data. Matrimid®5218 was purchased from Huntsman. SBAD-1 and DUCKY-9 polymers were prepared by the synthesis procedures as reported previously [28,29]. All chemicals (p-xylylene diamine, lithium nitrate, chloroform, tetrahydrofuran, 1-methylpyrrolidone, ethanol, methanol, hexane, toluene, 1,3,5-triiso-propyl benzene, n-octane, and iso-octane) were from Sigma Aldrich, Alfa Aesar, or TCI and used as received.

#### 2.2. Methods

# 2.2.1. Polymer membranes used for the separation performance trade-off plots in this work

The list of the polymer membranes used in this work contains linear polymer membranes that have been widely used for gas separation and organic solvent separations. The polymer membranes have also been used for an ML-based gas permeability model [24] and the ML organic solvent diffusion and sorption models (used in this work) [23]. The models are available at Polymer Genome (https://www.polymergenome.org/) – a web-based online platform. A total of 857 polymers were used in this work and the chemical structures of the polymers are provided in the Appendix of the Supporting Information file and in the Supplementary Data file.

# 2.2.2. ML predictions for pure organic solvent diffusion and sorption in polymers

The ML models for predicting solvent diffusion and sorption were employed to estimate the diffusivities (cm<sup>2</sup>/s) and sorption uptakes (mmol of solvent per gram of polymer) of toluene, n-octane, iso-octane, and TIPB in all 857 polymers investigated in this study [23]. These models were developed in our previous work, but re-trained with a small set of additional data that has been revealed after the publication, comprising 2066 datapoints (77 polymers, 151 solvents) for the ML diffusion model and 2296 datapoints (50 polymers, 91 solvents) for the ML sorption model. The full training sets are provided in the Supplementary Data file. The input features to the ML models included the chemical structures of polymers and solvents (based on SMILES, simplified molecular input line entry system) and solvent activity (e.g., unity value). The models output diffusivity (cm<sup>2</sup>/s) and sorption uptake (mmol of solvent per gram of polymer) at unit activity. Considering the uncertainties in ML predictions, it is possible to attempt propagating the uncertainties in the transport modeling conducted in this work. However, due to the extensive data utilized throughout this work involving a total of 857 polymer membranes and the fact that the average values predicted by the ML models are derived as the most probable prediction outcomes, this work used only the average of the ML predictions in the transport modeling. All ML predictions are also provided in the Supplementary Data file.

## 2.2.3. Maxwell-Stefan (MS) transport modeling for OSRO

A Maxwell-Stefan (MS) framework was employed to predict membrane performance in this work [21,22]. The MS equations governing solution-diffusion permeation are briefly shown in Eqs. (1)–(3).

$$(N^{V}) = -[B]^{-1}[\Gamma] \frac{d(\phi_{1:n}^{m})}{dz}$$
(1)

$$[B]_{ii} = \sum_{j=1:j\neq i}^{j=n} \frac{\phi_j^m}{\mathbf{D}_{ij}^{v,m}} + \frac{\phi_{n+1}^m}{\mathbf{D}_{i,n+1}^{v,m}}; \ [B]_{ij,i\neq j} = -\frac{\phi_i^m}{\mathbf{D}_{ij}^{v,m}}$$
 (2)

$$\Gamma_{ij} = \frac{\phi_i^m}{f_i^m} \frac{\partial f_i^m}{\partial \phi_j^m} = \phi_i^m \frac{\partial \ln f_i^m}{\partial \phi_j^m} = \phi_i^m \frac{\partial \ln \left( f_i^m / f_i^c \right)}{\partial \phi_j^m} = \phi_i^m \frac{\partial \ln \alpha_i^m}{\partial \phi_j^m}$$
(3)

Here, the indices 1 through n refer to n components permeating

through the membrane, while the membrane itself is represented as the  $(n+1)^{st}$  component. The superscript m denotes the membrane phase. The vector  $(N^V)$  is an  $(n \times 1)$  dimensional partial volumetric flux vector, [B] is an  $(n \times n)$  dimensional diffusion matrix, whose formulation is described in the following paragraphs.  $[\Gamma]$  is an  $(n \times n)$  dimensional sorption coupling matrix. The term  $\frac{\mathrm{d}(\phi_{1:n}^m)}{\mathrm{d}z}$  represents the  $(n\times 1)$  vector of volume fraction gradients across the membrane thickness (dz), with z =0 at the upstream feed-membrane interface and  $z = \ell$  at the downstream permeate-membrane interface.  $\phi_i^m$  is the volume fraction of permeating species *i* and  $\phi_{n+1}^m$  is the volume fraction of the polymer membrane; these volume fractions represent the volume of species relative to the total volume of the polymer-solvent system, which are obtained by unit conversion of sorption uptake (mmol of solvent per gram of polymer) predicted by the ML sorption model [23].  $f_i^m$  and  $f_i^c$  denote the fugacity of component i in the membrane phase and at the reference state, respectively.  $a_i^m$  represents the activity of sorbed species i in the membrane. Further details of the  $\Gamma$  matrix construction using predicted sorption uptakes (mmol of solvent per gram of polymer) from the ML sorption model and the Flory-Huggins sorption model and the solution procedure for the Maxwell-Stefan equations are available elsewhere [21,

In the [B] matrix in Eq. (2),  $D_{i,n+1}^{v,m}$  denotes the volume-based MS diffusivity of pure component i in the membrane. This quantity is obtained from mole-based Fickian diffusivity  $(D_{i,n+1}^m)$  predicted from the ML diffusion model used in this work. The mole-based Fickian diffusivity is related to the volume-based Fickian diffusivity  $(D_{i,n+1}^{v,m})$  by  $D_{ij}^m = \frac{D_{ij}^{v,m} \hat{V}}{V_j}$ , where  $\overline{V}_j$  is the partial molar volume of component j and  $\hat{V}$  is the molar volume of mixture by  $\hat{V} = \sum_{j=1}^{j=n+1} x_j^m \overline{V}_j$ . Then, the volume-based Fickian diffusivity  $(D_{i,n+1}^{v,m})$  is then thermodynamically corrected to the volume-based MS diffusivity  $(D_{i,n+1}^{v,m})$  by  $D_{i,n+1}^{v,m} = D_{i,n+1}^{v,m} \frac{\partial \ln(q_i^m)}{\partial \ln(q_i^m)}$ . In Eq. (2),  $D_{ij}^{v,m}$  is the mutual diffusion coefficient for the diffusional cross-coupling between molecules permeating through the membrane. The mutual diffusion coefficient is estimated by using the Vignes correlation, Eq. (4)

$$\frac{\mathbf{D}_{ij}^{\mathrm{v,m}}}{\overline{V}_{j}} = \left(\frac{\mathbf{D}_{i,n+1}^{\mathrm{v,m}}}{\overline{V}_{i}}\right)^{\frac{\phi_{i}^{m}}{\phi_{i}^{m}+\phi_{j}^{m}}} \left(\frac{\mathbf{D}_{j,n+1}^{\mathrm{v,m}}}{\overline{V}_{j}}\right)^{\frac{\phi_{i}^{m}}{\phi_{i}^{m}+\phi_{j}^{m}}} \tag{4}$$

The application of Eq. (4) implies that polymer membrane preserves distinct diffusivities for individual permeants, and thus enables separation based on diffusivity difference as well as sorption difference.

However, polymer membrane exposed to organic solvents may undergo plasticization and swelling, leading to loss of diffusivity-based selectivity so that the separation becomes dominated by sorption differences alone [22,33]. To model this transition, diffusivities are averaged based on the volume fractions as in Eq. (5), and a transition factor Y is introduced in Eq. (6) to interpolate between the Vignes-type diffusion modality that assumes fully preserved individual diffusivities and another diffusion modality that assumes complete loss of diffusivity selectivity as a function of chemical affinity between the polymer and the membrane (which is quantified by the Hansen solubility difference,  $R_a$ , in unit of MPa $^{0.5}$  by Eq. (7)).

$$\mathbf{\mathfrak{D}}_{i,n+1,averaged}^{v,m} = (\overline{V}_i)^{-1} \prod_{k=1}^{n} \left( \mathbf{\mathfrak{D}}_{i,n+1}^{v,m} \overline{V}_k \right)^{\frac{\phi_k^m}{n}} \phi_j^m$$
 (5)

where, 
$$Y = \frac{1}{2} \cdot \left[ \tanh \left\{ c \cdot \left( R_a - 8 MPa^{0.5} \right) \right\} + 1 \right]$$

$$R_{a}^{2} = 4 \cdot \left(\delta_{D,mixture} - \delta_{D,polymer}\right)^{2} + \left(\delta_{P,mixture} - \delta_{P,polymer}\right)^{2} + \left(\delta_{H,mixture} - \delta_{H,polymer}\right)^{2}$$

$$(7)$$

where  $\delta_{mixture}$  and  $\delta_{polymer}$  are the Hansen solubility parameters of mixture and polymer, respectively. The subscripts D, P, and H refer to dispersion, polarity, and hydrogen bonding components. The Hansen solubility parameters for the mixture are calculated in the following way:

$$\delta_{A,mixture}^2 = \sum_{j=1}^{n} \frac{\phi_j^m}{1 - \phi_{n+1}^m} \delta_{A,j,pure}^2 \text{ where } A = D, P, and H$$
 (8)

Here,  $\delta_{A,mixture}$  and  $\delta_{A,j,pure}$  represent the solubility parameters of the mixture and component j in unit of MPa<sup>0.5</sup>, respectively. Subscript A is used to describe three solubility factors: dispersion (D), polarity (P), and hydrogen-bonding (H).  $\phi_j^m$  and  $1-\phi_{n+1}^m$  denote the volume fractions of component j and the entire mixture in the membrane phase each.

When  $R_a$  is much larger than 8 MPa<sup>0.5</sup> (indicating weak chemical affinity between the polymer membrane and the mixture), the diffusion transition factor Y approaches 1, and the original individual diffusivities are preserved, maintaining separation based on diffusivity difference. In such case, there is no distinction between the new diffusivity ( $\Phi^{v,m}_{i,n+1,new}$ ) and the original diffusivity ( $\Phi^{v,m}_{i,n+1}$ ). Conversely, as  $R_a$  decreases toward 0, the diffusion transition factor Y approaches 0, diffusivities converge to a single value calculated by Eq. (5), leading to sorption-driven separation with no diffusion selectivity. For intermediate  $R_a$  values, diffusivities transition smoothly between the two different diffusion modalities according to Y (Eq. (6)).

A critical factor in this context is the constant c in Eq. (6). The constant c controls the steepness of this transition as a function of  $R_a$  and is referred to as the "steepness constant" or "plasticization resistance constant" (Fig. S2) [21]. Larger c values (e.g., 0.5) imply stronger resistance to plasticization, preserving diffusion-based separation even at moderate chemical affinities, while smaller c values (e.g., 0.1) imply greater susceptibility to plasticization. Prior work has shown reasonable prediction accuracy for c values between 0.1 and 0.5 for different polymer classes (e.g., polyimide, spirocyclic hydrophobic polymers), but no universal single value has been established [21]. The constant may be varied across different polymer and solvent classes. Therefore, this study performed separation predictions using c = 0.1, 0.3, and 0.5 and also reported the arithmetic averaged of the prediction results, with full data provided in the Supplementary Data file. For all predictions conducted in this work, a temperature of 295 K and an upstream pressure of 50 bar and a downstream pressure of 1 bar were always assumed. In addition, membrane thickness was always assumed to be 1  $\mu$ m.

2.2.4. Application of a data-driven solvent/non-solvent classification model

The objective of this work is to identify potential landscapes (or trade-off plots) that reflect the potential of known polymer membranes for use in OSRO separations. While including a large number of polymer cases is essential for exploring broad chemical spaces, it is also important to account for practical issues inherent to polymer membrane applications in organic solvent separations, such as the risk of dissolution, swelling, and even plasticization. When polymeric materials are employed as membranes, dissolution or excessive swelling can occur depending on polymer-solvent interactions, potentially undermining separation performance. To account for this, a solvent/non-solvent classification model developed previously [34,35] and implemented in PolymRize, a web-based platform (https://polymrize.matmerize.com) was used for pre-screening polymer candidates for these mixture separations. This model provides a solvent-likelihood score for 58 organic liquids with respect to a given polymer, ranging from -1 (non-solvent) to +1 (strong solvent). For example, a score of +0.5 for toluene with respect to a given polymer implies approximately a 50 % probability that toluene would act as a solvent for that polymer. By using this model, polymers were excluded from performance predictions if the main component of the mixture exhibited a solvent-likelihood score above 0.5. Specifically, toluene was used as the criterion for the toluene/TIPB and toluene/iso-octane systems, and heptane was used as a surrogate for n-octane/iso-octane, as n-octane was not included in the model's database. Although solvent strength may be attenuated in a mixture due to co-solvent interactions, dissolution remains a critical risk when a strong solvent is present; therefore, this screening was based solely on the predicted score of the primary solvent. The prediction results are provided in the Supplementary Data file. As a result of this pre-screening step, 491 polymers were excluded from the toluene/TIPB and toluene/iso-octane separation analyses, and 415 polymers were excluded from the n-octane/iso-octane analysis.

### 2.2.5. Liquid mixture permeation measurement

Y.J. Lee et al.

Thin film composite (TFC) membranes for liquid mixture permeation tests were fabricated by spin coating polymer materials (Matrimid, SBAD-1, and DUCKY-9) onto a cross-linked, porous polyimide (Matrimid) support film. The preparation of the support films and the TFC membranes with the selective layer was performed according to previously established methods [23,29]. Briefly, Matrimid powders (16 wt%) and lithium nitrate (LiNO3, 3 wt%) were dissolved in a solvent mixture consisting of 1-methyl-2-pyrrolidone (69 wt%), tetrahydrofuran (10 wt %), ethanol (1 wt%), and deionized water (1 wt%). Prior to dissolution, the solid powders (Matrimid and LiNO<sub>3</sub>) were dried under vacuum at 110 °C. The solution was then mixed on a roller for two days to ensure complete dissolution. The resulting polymer solution was cast onto a glass plate using a 10 MIL doctor blade, and after 10 s, it was rapidly transferred to a water bath to induce a non-solvent phase inversion process. The cast support films were immersed in deionized water for three days and underwent three successive solvent exchanges in methanol and hexane at 2 h-interval. The films were then air-dried for 1 h and cut into circular coupons with an effective area of 10.25 cm<sup>2</sup>. Following this, cross-linking was achieved by immersing the support films in a solution of 5 g of p-xylene diamine dissolved in 100 ml of methanol for 24 h, followed by the same solvent exchange process with methanol and hexane to remove any residual cross-linker. The final supports were stored in hexane and air-dried for 24 h prior to use.

To fabricate the TFC membranes for this study, a polymer dope solution (1 wt% polymer in chloroform) was spin-coated onto the crosslinked polyimide support. Each polymer solution, stored at 5  $^{\circ}$ C, was dispensed (0.7 ml) onto the support film located on a plate in a spin coater, operating at 1200 rpm. The spin coater chamber was saturated with chloroform vapor by placing cotton soaked in chloroform and introducing dry N<sub>2</sub> gas. The resulting TFC membranes were air-dried for 24 h before further testing.

Liquid permeation tests were carried out in a custom-built cross-flow system pressurized up to 50 bar on the upstream side by an HPLC pump (Azura P 4.1S, Knauer) at 295 K [21]. The feed flow rate was maintained consistently at a 15 ml/min such that the stage cut was <3%. The tested mixtures were toluene/iso-octane mixture with concentrations of 90/10 (mol %), 80/20 (mol %), and 70/30 (mol %), and n-octane/iso-octane with a concentration of 90/10 (mol %). The concentration of the permeate was analyzed by gas chromatography (7890B GC, Agilent) and the separation factor was calculated as the following way:

$$Separation \ factor_{Tolluene/TIPB} = \frac{C_{p,Tolluene}}{C_{f,Tolluene}} \times \frac{C_{f,TIPB}}{C_{p,TIPB}}$$

where  $C_{p,Toluene}$  and  $C_{f,Toluene}$  are the permeate and feed concentration of toluene, and  $C_{p,TIPB}$  and  $C_{f,TIPB}$  are the permeate and feed concentration of TIPB. The experiments were typically run for more than 2–3 days to allow for steady state permeation profiles to develop. For the mixture permeation tests, different thin film composite samples were tested in triplicate. All permeation tests were predicted by the Maxwell-Stefan

model described in this work.

#### 3. Results and discussion

In this work, three representative binary liquid hydrocarbon mixtures were investigated: toluene/TIPB, toluene/iso-octane, and n-octane/iso-octane, corresponding to aromatic, aromatic/aliphatic, and aliphatic separations, respectively. The toluene/TIPB mixture is a widely used benchmark for evaluating polymer-based OSRO membranes. The toluene/iso-octane mixture is industrially relevant due to environmental regulations requiring reduced aromatic content in gasoline [36,37]. Conventional separation methods, such as distillation, are hindered by close boiling points (110.6  $^{\circ}\text{C}$  for toluene and 99  $^{\circ}\text{C}$  for iso-octane) and azeotropic behavior [38-40], while alternative techniques (i.e., extractive distillation) are costly and solvent-intensive [38, 41]. The n-octane/iso-octane mixture represents linear/branched alkane separation, critical for upgrading gasoline octane ratings [42]. Conventional thermal and chromatographic methods for this separation are energy-intensive [43-45], and membrane-based separation technologies such as OSRO have potential as an alternative.

This work explored the potential separation performance of polymer membranes for the three representative OSRO-based binary hydrocarbon separations, accounting for key factors that constrain practical applications. Specifically, the study exmained the effects of polymer dissolution and plasticization on separation performance landscape (trade-off) plots, the reduction in achievable membrane productivity due to permeation resistance in the support layer, and the separation efficiency limits imposed by osmotic pressure when separation highly concentrated mixtures beyond the dilute concentration ranges typically used in material testing.

#### 3.1. Accounting for polymer plasticization and dissolution

Predicted separation performances for the 857 polymer membranes were evaluated for the three binary hydrocarbon mixtures, toluene/ TIPB (95/5 mol%), toluene/iso-octane (90/10 mol%), and n-octane/isooctane (90/10 mol%), as shown in Fig. 1a, b, and 1c. For these predictions, a plasticization constant (c) of 0.5 in Eq. (6) was assumed and no mass transfer resistance in the support layer was assumed in the predictions. It is important to note that these plots report the permeance of the main solvent component in each mixture (toluene for the toluene/ TIPB and toluene/iso-octane mixture, and n-octane for n-octane/isooctane mixture) and the corresponding separation factor rather than simply the ratio of pure-component permeabilities and ideal permselectivity. For all three mixture separation cases (Fig. 1a, b, and 1c), a general trade-off was observed; polymers exhibiting higher permeance tend to show lower separation factors, and vice versa. Among the three separation cases, the toluene/TIPB separation exhibits the highest potentially achievable separation factors, likely due to the large molecular weight differences among toluene (92.14 g mol<sup>-1</sup>), and TIPB  $(204.35 \text{ g mol}^{-1})$ , and octanes  $(114.23 \text{ g mol}^{-1})$ , which may enhance both diffusion and sorption selectivity.

While these predictions (Fig. 1a, b, and 1c) were made for all 857 polymers, it must be considered that polymers may dissolve when exposed to the target organic solvent mixture, rendering them unsuitable for OSRO membrane applications. To account for this, a solvent/non-solvent classification model implemented in PolymRize was used to pre-screen polymers. Polymers for which the main component of the mixture was predicted to behave as a strong solvent (i.e., solvent-likelihood probability >50 %) were identified (also provided in the Supplementary Data file). As shown in Fig. 1a, b, and 1c, 491 polymers were predicted to have a high likelihood of dissolution in toluene and 415 polymers in heptane. These polymers (cyan triangles in the plots) generally exhibited higher permeance than those predicted to be unlikely dissolved (red circles in the plots). Although both separation performance predictions and the solvent/non-solvent classification

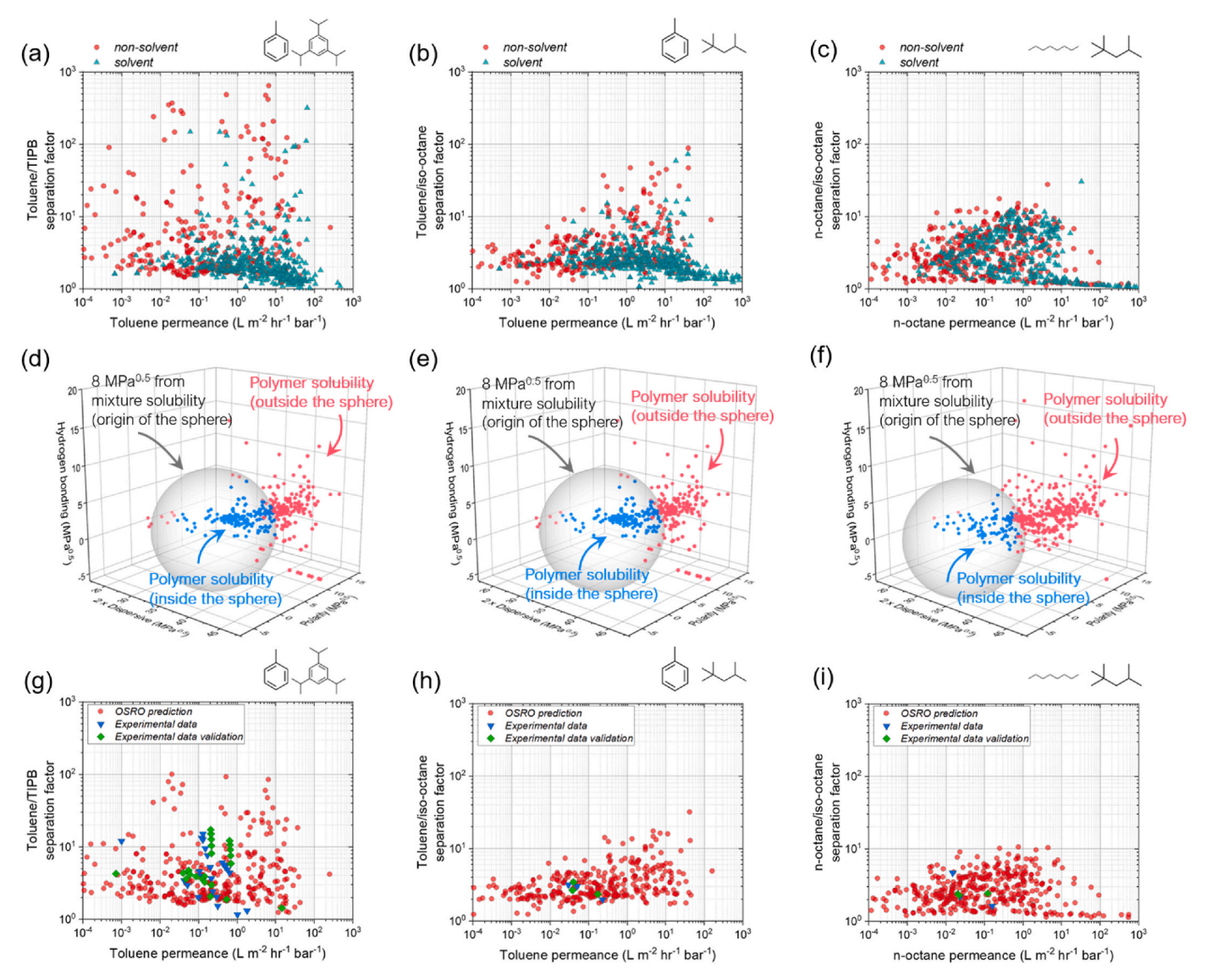


**Fig. 1.** OSRO separation performance predictions for 857 polymers for (a) toluene/TIPB (95/5 mol%), (b) toluene/iso-octane (90/10 mol%), and (c) n-octane/iso-octane (90/10 mol%). Red circles indicate polymers for which the main solvent is predicted to act as a non-solvent, while cyan triangles indicate polymers for which the main solvent is predicted to act as a strong solvent. Among the 857 polymers, 491 and 415 polymers were predicted to have toluene and heptane (used as a surrogate for n-octane), respectively, as strong solvents. Hansen solubility parameters of the test hydrocarbon mixtures and the 857 polymers are shown for (d) toluene/TIPB, (e) toluene/iso-octane, and (f) n-octane/iso-octane. The sphere represents the locus of points at a distance of 8 MPa<sup>0.5</sup> from the test mixture at the origin. Polymers with a solubility difference from the mixture less than 8 MPa<sup>0.5</sup> (i.e., located within the sphere) are shown as blue dots (179, 169, and 99 polymers for toluene/TIPB, toluene/iso-octane, and n-octane/iso-octane, respectively). Polymers with a solubility difference greater than 8 MPa<sup>0.5</sup> (i.e., located outside the sphere) are shown as red dots (187, 197, and 343 polymers, respectively). Separation performance plots including only the average predictions across three different c values are shown for (g) toluene/TIPB, (h) toluene/iso-octane, and (i) n-octane/iso-octane; here, polymers for which the main solvent was classified as a strong solvent by the solvent/non-solvent classification model were excluded. In panels (g), (h), and (i), blue inverted triangles represent the experimentally measured separation performance of previously reported linear polymer membranes, while the light green diamonds indicate the corresponding predictions by the model used in this work (Fig. S7 and Table S1). (For interpretation of this article.)

predictions are data-driven and carry some potential uncertainties, polymers at high dissolution risk were excluded from subsequent analyses to derive reliable and possible OSRO separation performance landscapes. The separation performance plots including only solvent-compatible polymers are provided separately (Fig. S3).

Even when a polymer membrane does not fully dissolve in a given mixture, plasticization may occur depending on the chemical affinity between the polymer membrane and the mixture, potentially degrading separation efficiency (i.e., separation factor). Fig. 1d, e, and 1f present the Hansen solubilities of polymers and each mixture, where smaller distance between polymer and mixture indicates stronger chemical affinity. Our prior work demonstrated that as the chemical affinity

between a polymer membrane and a mixture increases, the likelihood of plasticization rises, leading to diminished separation selectivity driven by the diffusivity difference [21]. To capture this phenomenon, Equations (4)–(6) were incorporated into the model, with chemical affinity quantitatively represented by the Hansen solubility difference ( $R_a$ ) in Eq. (7). In particular, it was shown previously that separation efficiency begins to degrade noticably when the Hansen solubility difference falls below approximately 8 MPa $^{0.5}$ .

The extent of this effect is captured in the model by the plasticization resistance constant, c, in Eq. (6), which reflects the membrane's resistance to plasticization: larger values imply greater resistance, allowing the membrane to maintain separation performance despite high

chemical affinity with the mixture (Fig. S2). In contrast, smaller values represent membranes that are more susceptible to performance loss due to plasticization. The prior study indicated that reasonable plasticization constant values may range from 0.1 to 0.5, but no universal value applicable to all polymer-mixture pairs has been established. Therefore, for the polymers that passed the initial solvent/non-solvent prescreening (Fig. 1a, b, and 1c), separation performances were predicted using three different plasticization resistance constant values (c = 0.1, 0.3, 0.5) (Figs. S4, S5, and S6). As the plasticization constant cdecreased, the predicted separation performance of polymers with initially high separation factors progressively declined. This trend was particularly pronounced for toluene/TIPB (Fig. S4) compared to toluene/iso-octane (Fig. S5) and n-octane/iso-octane (Fig. S6), likely due to the larger molecular size difference between toluene and TIPB, which enhances separation based on diffusivity difference, but also makes it more vulnerable to plasticization if the membrane lacks sufficient plasticization resistance.

Predictions for previously reported linear polymer membranes for toluene/TIPB [28,29,46-48], and SBAD-1, Matrimid, and DUCKY-9 for toluene/iso-octane and n-octane/iso-octane (which were newly tested in this work) were compared across different c values (Fig. S7 and Table S1–S3). These comparisons reveal that the c value yielding the best agreement between predicted and experimental separation factors varies depending on polymer and mixture class, indicating that plasticization resistance may be polymer- and solvent-specific. Therefore, we speculate that no single c value can be universally applied. However, c values between 0.1 and 0.5 generally produced excellent prediction accuracy, both in this work and in a prior study [21]. Accordingly, the separation performance plots in Fig. 1g, h, and 1i report the arithmetic averages of the predicted separation performance across the three c values (0.1, 0.3, 0.5) to present a more balanced and realistic performance landscape. Notably, the top-performing polymers identified in Fig. 1g, h, and 1i show superior separation performance, achieving higher separation factors and permeances than previously reported polymer membranes (represented by green diamonds and blue inverted triangles in the plots). As a result of the modeling, polymer structures exhibiting both high permeance and separation efficiency (top 20 by separation factor in each hydrocarbon separation case, with permeance above 0.5 L m<sup>2</sup> hr<sup>-1</sup> bar<sup>-1</sup>) were identified across the three hydrocarbon mixtures examined in this work (Fig. S8). In particular, spirocyclic polymers with polar groups such as esters incorporated in the backbone and polyimides with ether functionalities were predicted to be especially promising for these separations. Experimental verification of these polymers will be needed in the future.

## 3.2. Permeation limited by mass transfer resistance in support layer

Asymmetric membranes such as thin film composite membranes (TFC), which consist of a thin selective layer ( $\sim\!100$  nm-1  $\mu m)$  coated on a porous support layer that possesses chemical and mechanical stability are practical for membrane applications. TFC membranes exhibit a high flux for gas, vapor, and liquid permeation and are viable for a wide range of applications. However, due to the mass transport resistance in the support layer, the high flux increases the importance of properties of the support layer.

When predicting OSRO performance, it is essential to consider the permeation resistance of the support layer used. In this context, several studies have modeled the resistance generated in each layer (coated skin layer and porous support layer) and the total resistance as a sum of these individual resistances [49–52]. A notable example is the permeation resistance model developed by Henis and Tripodi [51], which was inspired by the resistance model of an electrical circuit (Fig. S9).

Inspired by this model, this work considered the resistance to permeation rate that may occur in the support layer in the use of a practical TFC format. However, contrary to previous work [51], there is currently no information about small pores such as those found in skin

layers or defects between the top selective skin layer and the highly porous support layer (Fig. S9). Therefore, to simplify the use of this model in transport modeling, it was assumed that the three distinct layers ( $R_2$ ,  $R_3$ , and  $R_4$  in Fig. S9) were consolidated into a unified virtual resistance layer, with the surface fraction set to 1 (Fig. 2).

The total permeation resistance ( $R_{TFC}$ ) and total permeance ( $\mathbb{P}_{TFC}/\ell_{TFC}$ ) through TFC membrane are formulated as follows:

$$R_{TFC} = R_{skin} + R_{support} \tag{9}$$

$$\frac{\ell_{TFC}}{\mathbb{P}_{TFC}} = \left(\frac{\ell_{skin}}{\mathbb{P}_{skin}} + \frac{\ell_{support}}{\mathbb{P}_{stupport}}\right) \tag{10}$$

where R is the resistance of the layer and  $\mathbb{P}$  is the permeability, and  $(\mathbb{P}/\ell)$  is the permeance  $(L \ m^{-2} \ hr^{-1} \ bar^{-1})$ . If the permeance of the support  $(\mathbb{P}_{support} / \ell_{support})$  is significantly low relative to the permeance in the skin layer  $(\mathbb{P}_{skin} / \ell_{skin})$ , the overall permeance of the TFC membrane becomes limited by the permeance of the support. On the other hand, if the permeance of the support is enormously high relative to the permeance of the skin layer, the TFC permeance is limited by the permeance of the dense skin layer (as desired).

In OSRO separations, ultrafiltration membranes with permeance of  $50-100 \,\mathrm{L\,m^{-2}\,hr^{-1}\,bar^{-1}}$ , or even that of up to  $1000 \,\mathrm{L\,m^{-2}\,hr^{-1}\,bar^{-1}}$  in exceptionally fast cases, are utilized as support materials. The crosslinked Matrimid support fabricated and used in this work exhibits permeance of approximately 50–100 L m<sup>-2</sup> hr<sup>-1</sup> bar<sup>-1</sup> with thickness of a 150-200 μm. The landscapes illustrating the variations in TFC membrane-based OSRO as influenced by the use of the permeation resistance model (Equations (9) and (10)) are shown in Fig. 3. For the study of potential permeance of TFC membranes, various ranges of maximum permeance values of the supports were employed:  $10~L~m^{-2}$ hr<sup>-1</sup> bar<sup>-1</sup> (range of nanofiltration membrane for the slowest support case), 50 and 100 L m<sup>-2</sup> hr<sup>-1</sup> bar<sup>-1</sup> (range of ultrafiltration membrane), and 1000 L m<sup>-2</sup> hr<sup>-1</sup> bar<sup>-1</sup> (range of microfiltration membrane as the fastest with minimal resistance support example). The resistance was integrated into TFC permeance calculations and no selectivity was assumed in the support layer; thus, the separation factor is not affected throughout the support layer.

As expected, for all mixtures, no predicted permeance values exceeded the maximum permeance determined by the permeation resistance in the support layer. The permeation resistance model used in this work assumed that the support layer imposes no selectivity, even for supports with low permeance (e.g.,  $10 \text{ L m}^{-2} \text{ hr}^{-1} \text{ bar}^{-1}$ ), typical of commercial nanofiltration membranes. However, in practice, nanofiltration-type supports could influence selectivity, particularly for molecules such as TIPB that lie near the upper molecular weight of OSRO target ( $<200 \text{ g mol}^{-1}$ ) and the lower limit of nanofiltration targets (200– $1000 \text{ g mol}^{-1}$ ). Thus, experimental results for these systems may deviate from predictions assuming non-selective supports.

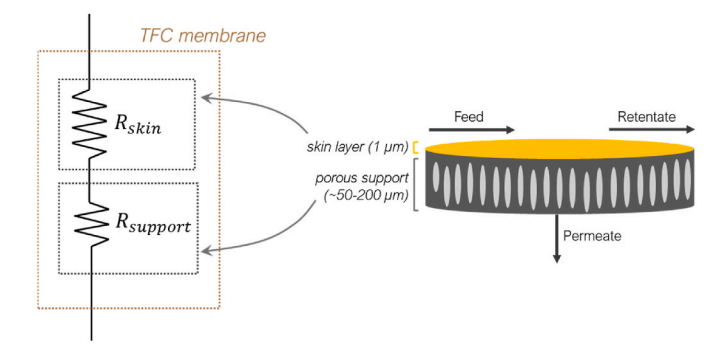


Fig. 2. Schematic representation of permeation resistance model used in this work.  $R_{skin}$  and  $R_{support}$  indicate the permeation resistance in the skin layer and support layer, respectively.

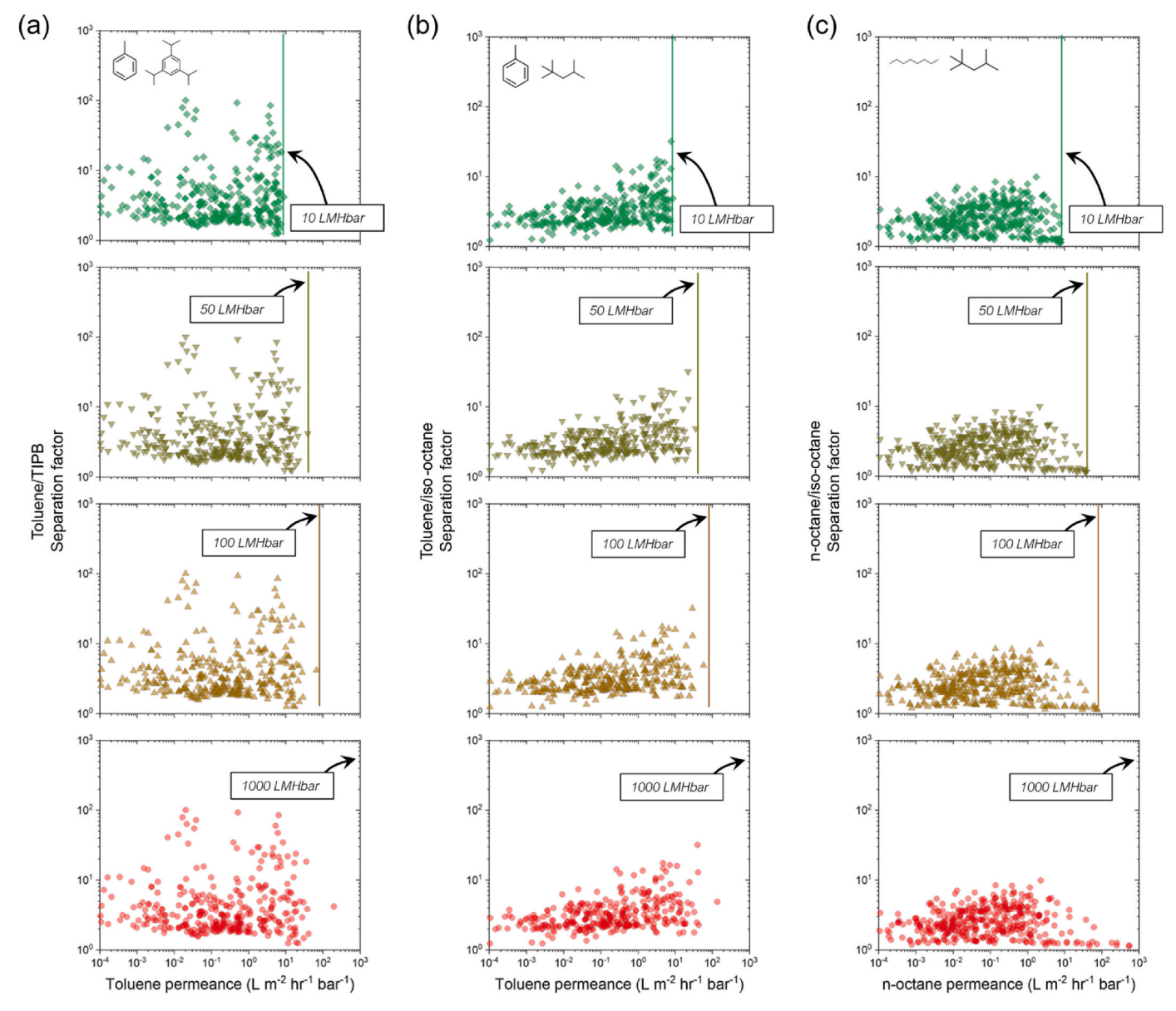


Fig. 3. Separation performance predictions for polymer membranes for (a) toluene/TIPB (95/5 mol%), (b) toluene/iso-octane (90/10 mol%), and (c) n-octane/iso-octane (90/10 mol%) with a permeation resistance model (Eqs. (9) and (10)). Each panel from top to bottom corresponds to different productivity thresholds: 10, 50, 100, and  $1000 \, \text{L m}^{-2} \, \text{hr}^{-1} \, \text{bar}^{-1}$  (LMHbar), respectively. Note that no influence of the support layer on the separation factor was assumed. Vertical lines indicate the specified support permeance in each plot. Only polymers passing the solvent compatibility screening (i.e., main solvent predicted to act as a non-solvent) are included.

For the toluene/TIPB and toluene/iso-octane mixtures (Fig. 3a and b), the fastest permeance, assuming a free-standing, defect-free dense polymer membrane of 1  $\mu m$  thickness, ranged from 10 to 200 L  $m^{-2}$  hr $^{-1}$  bar $^{-1}$ , although a few polymers exhibited that high permeance. Imposing a support resistance typical of ultrafiltration membranes (50–100 L  $m^{-2}$  hr $^{-1}$  bar $^{-1}$ ) or even higher (1000 L  $m^{-2}$  hr $^{-1}$  bar $^{-1}$ ) produced minimal changes in the separation performance landscape. In contrast, for the n-octane/iso-octane mixture separation (Fig. 3c), a relatively larger number (still a few polymers) of polymers were predicted to exceed 100 L  $m^{-2}$  hr $^{-1}$  bar $^{-1}$  although with separation factors close to unity, indicating marginal selectivity. For these cases, support layer resistance could substantially limit achievable permeance.

While this work consistently assumed a 1  $\mu m$  membrane thickness, practical membrane fabrication often seeks thinner selective layers (~100 nm) to achieve higher flux or permeance. Theoretically, permeance increases inversely with membrane thickness, necessitating highly permeable support to minimize support layer resistance (i.e.,

 $1000~L~m^{-2}~hr^{-1}~bar^{-1}$ ). Achieving such high permeance typically requires enlarging support pore sizes, which introduces challenges in forming defect-free, dense skin layers, as excessive pore sizes can lead to solution infiltration and caulking during coating [53,54]. This condition may result in observed performance that reflects a combination of the polymer coating and the underlying support rather than the true intrinsic separation capability of the polymer membrane. Furthermore, highly porous supports often suffer from inadequate mechanical strength, limiting their suitability for high pressure OSRO applications ( $\sim\!100~bar$ ). These considerations also extend to integrally skinned asymmetric membranes where the dense skin layer and porous support are formed from a single polymer [55]. An alternative approach involves increasing the surface porosity of supports while maintaining small pore sizes, potentially facilitating both mechanical robustness and the formation of high-quality selective layers.

# 3.3. Effect of mixture concentration on membrane-based OSRO separations

According to the thermodynamic entropy law of diffusion, molecules are driven to diffuse from a region of high concentration to a region of low concentration. When a polymer membrane selectively separates a specific molecule or more in a mixture, osmotic pressure is formed for the solvent (the more permeable molecule in the case of a binary mixture). This osmotic pressure is determined by the concentrations of feed fluid and permeate fluid (Equation (11)) as below:

$$\pi \; (\textit{osmotic pressure}) = -\frac{RT}{\hat{V}_i} \cdot \ln \left[ \frac{x_i^{\textit{feed}} y_i^{\textit{feed}}}{x_i^{\textit{permeate}} y_i^{\textit{permeate}}} \right] \tag{11}$$

where R is the gas constant (8.3145 J/mol/K),  $x_i^{feed}$  and  $x_i^{permeate}$  are the mole concentrations of component i, and  $\gamma_i^{feed}$  and  $\gamma_i^{permeate}$  are the activity coefficients of component i at feed and permeate stream, respectively. Assuming perfect separation, the lower the solvent concentration (the greater the solute concentration), the higher osmotic pressure, necessitating a sufficiently high transmembrane pressure to counteract the osmotic pressure in the OSRO-based separation process. Regardless of the selectivity that can be exhibited by the membrane, achieving a permeate concentration that generates osmotic pressure exceeding the

applied transmembrane pressure is difficult (Fig. 4a). However, in industrial applications, mixture concentrations span the entire range from dilute to concentrated. Consequently, the concentration of a given mixture can significantly impact the landscape of separation properties for polymer membrane-based OSRO.

This work also investigated the effect of feed mixture concentration on OSRO separations for the three binary hydrocarbon mixture classes (toluene/TIPB, toluene/-iso-octane, and n-octane/iso-octane) (Fig. 4b, c, and 4d). In the predictions, all parameters including 50 bar pressure applied at the upstream side were applied consistently, and the concentrations of toluene/TIPB mixture were 95/5 mol%, 90/10 mol%, and 80/20 mol%, while the concentrations of toluene/iso-octane mixture and n-octane/iso-octane mixture were changed from 90/10 mol% to 80/20 mol%, 70/30 mol% and 60/40 mol%. The osmotic pressure that could occur, assuming perfect separation (i.e., the permeate is pure solvent with no solute molecule), for each mixture concentration was calculated using Equation (11), and is listed in Table S4.

In the case of toluene/TIPB mixture (Fig. 4b), even when assuming perfect separation at concentrations of 95/5 mol% and 90/10 mol%, the osmotic pressure exerted by the toluene solvent across the membrane is substantially lower than the applied transmembrane pressure of 50 bar (Table S4), resulting in an effective driving force (activity gradient) and achieving a high degree of separation efficiency. As the feed

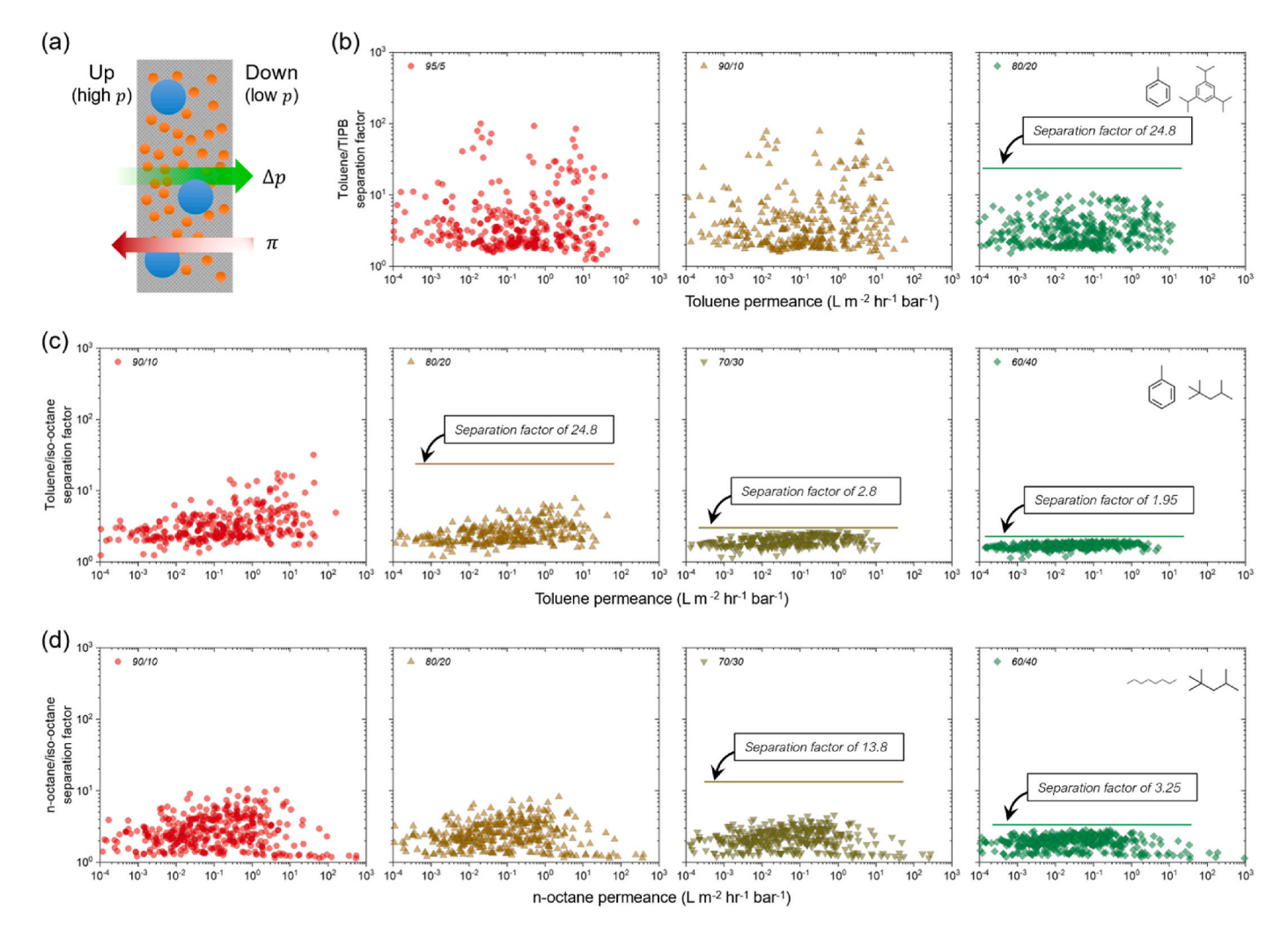


**Fig. 4.** (a) Schematic illustration of transmembrane pressure ( $\Delta p$ ) and opposing osmotic pressure ( $\pi$ ) in membrane separations. Predicted separation performances for (b) toluene/TIPB, (c) toluene/iso-octane, and (d) n-octane/iso-octane mixtures under varying feed concentrations. For toluene/TIPB, feed concentrations range from 95/5 to 80/20 mol%, while for toluene/iso-octane and n-octane/iso-octane, feed concentrations range from 90/10 to 60/40 mol%. Within each row, plots are arranged from left to right in order of decreasing main component concentration (i.e., increasing solute concentration). An applied transmembrane pressure of 50 bar ( $\Delta p$ ) was assumed for all cases.

concentration changes, the activity gradient (driving force of molecular diffusion) within the membrane also changes, leading to variations in the separation capability and permeance. However, since the given transmembrane pressure still exceeds the osmotic pressure in the cases of these two mixture concentrations, no significant difference in separation is predicted. However, when the concentration becomes 80/20 mol%, the osmotic pressure with the assumption of perfect separation reaches around 51.6 bar (Table S4), exceeding the transmembrane pressure. Consequently, a less effective activity gradient can be established, leading to a sharp decline in separation efficiency. The permeate concentration, which generates an osmotic pressure equal to the applied transmembrane pressure, was calculated, and the corresponding separation factor was determined to be 24.8. It is evident that this high osmotic pressure acts as a thermodynamic resistance to separation.

In the toluene/iso-octane mixture separation cases (Fig. 4c), when the feed concentration is 90/10 mol%, the osmotic pressure with the assumption of perfect separation is 24.3 bar, which is noticeably lower than the applied transmembrane pressure. As a result, the separation resistance due to osmotic pressure is relatively low, resulting in high separation selectivity, as illustrated in the figure. However, as the concentration of the solvent (toluene in this case) decreased to 80 mol%, 70 mol% and 60 mol %, the osmotic pressure of perfect separation scenario rises to 51.6 bar, 82.5 bar, and 118.2 bar, respectively (Table S4), exceeding the applied transmembrane pressure. In such cases, the osmotic pressure formed across the membrane is likely to act as a significant resistance to selective separation. Accordingly, as shown in Fig. 4c, a dramatic decrease in the predicted separation factors was observed as the concentration of the toluene solvent in the feed decreased. In these, permeation concentrations to generate osmotic pressures equal to the applied transmembrane pressure were calculated; thereby, the separation factors predicted for the polymer membranes do not exceed the theoretical limits of 24.8, 2.8, and 1.95 with the feed concentration of 80/20 mol%, 70/30 mol%, and 60/40 mol%, respectively.

In the case of n-octane/iso-octane mixture separations (Fig. 4d), the applied transmembrane pressure exceeds the perfect separation-based osmotic pressures of 15.9 bar and 33.7 bar with solvent (n-octane in this case) concentrations of 90 mol% and 80 mol% (Table S4). Due to the effective transmembrane pressures and induced activity gradients in these cases, high separation efficiency is still anticipated. As the concentration of the mixture reaches 70/30 mol% and 60/40 mol%, the osmotic pressure formed in complete separation assumption begins to surpass the transmembrane pressure; therefore, the limit separation factors of 13.8 and 3.25 are calculated, and the separation factors achieved by the polymers do not exceed the theoretical limit. In the cases of toluene/iso-octane and n-octane/iso-octane separations, at high solute concentration (e.g., 60/40 mol%), high separation factors cannot be achieved due to inherent thermodynamic limitations imposed by osmotic pressure. When the mechanical strength of membranes and modules constrains the maximum applied pressure, such that it cannot be increased indefinitely, the system must operate under reduced effective driving force at high osmotic pressure. Under such conditions, it may be more rational to select polymer membranes exhibiting intrinsically high permeability rather than those demonstrating high selectivity at low solute concentrations, as the achievable separation factor is fundamentally limited by the osmotic pressure.

# 4. Conclusion

In this study, the landscapes of polymer-membrane-based organic solvent reverse osmosis separation processes for three representative hydrocarbon mixtures were investigated. Diffusivities and solubilities of pure organic liquid molecules predicted via machine algorithms were parameterized into Maxwell-Stefan permeation equations coupled with the Flory-Huggins sorption models. To develop a practical polymer membrane-based OSRO landscape, variables that account for the plasticization resistance of polymer membranes to the hydrocarbon mixtures

(plasticization resistance constant), permeation resistance in the porous support layer (via the permeation resistance model), and separation efficiency constrained by osmotic pressure relative to feed mixture concentration were integrated into the landscape.

While this study focused on three representative binary hydrocarbon mixtures, the modeling framework used in this work can readily be applied to a wide variety of binary and more complex organic solvent mixtures that require energy-efficient separation. Although approximately 800 polymer membranes were explored in this work, this set does not comprehensively represent the full diversity of polymeric materials, and expanding this investigation to a broader range of polymers would be an interesting and important direction for future research. Moreover, as the separation performance landscapes presented in this study are based on predictive models, experimental validation – at least for a subset of the predictions that are not experimentally validated in this work – will be essential to confirm the reliability and applicability of the proposed approach.

#### CRediT authorship contribution statement

Young Joo Lee: Writing – review & editing, Writing – original draft, Software, Methodology, Formal analysis, Conceptualization. Janhavi Nistane: Writing – review & editing, Visualization, Software, Data curation. Rampi Ramprasad: Writing – review & editing, Supervision, Funding acquisition. Ryan P. Lively: Writing – review & editing, Writing – original draft, Supervision, Resources, Project administration, Methodology, Funding acquisition, Conceptualization.

#### **Declaration of competing interest**

RR is the co-founder of Matmerize, Inc., a polymer informatics software company that created the PolymRize software. All other authors declare no competing interests.

# Acknowledgement

Y. J. L. acknowledges his fellowship from Kwangjeong Educational Foundation (South Korea). This work was supported by ExxonMobil Technology and Engineering Company. We thank Nicholas C. Bruno, Valentino Perez, and M. G. Finn for providing DUCKY-9 and SBAD-1. We thank Dr. Wenjun Li (ExxonMobil Technology and Engineering Company) for providing the HSP parameters.

# Appendix A. Supplementary data

Supplementary data to this article can be found online at https://doi.org/10.1016/j.polymer.2025.129153.

# Data availability

All data relevant to this article is provided in the main text, the Supporting Information file, and the Supplementary Data file.

#### References

- L.M. Robeson, The upper bound revisited, J. Membr. Sci. 320 (1–2) (2008) 390–400.
- [2] H. Lin, M. Yavari, Upper bound of polymeric membranes for mixed-gas CO2/CH4 separations, J. Membr. Sci. 475 (2015) 101–109.
- [3] M.M. Dal-Cin, A. Kumar, L. Layton, Revisiting the experimental and theoretical upper bounds of light pure gas selectivity-permeability for polymeric membranes, J. Membr. Sci. 323 (2) (2008) 299–308.
- [4] G.M. Geise, H.B. Park, A.C. Sagle, B.D. Freeman, J.E. McGrath, Water permeability and water/salt selectivity tradeoff in polymers for desalination, J. Membr. Sci. 369 (1–2) (2011) 130–138.
- [5] A. Mehta, A.L. Zydney, Permeability and selectivity analysis for ultrafiltration membranes, J. Membr. Sci. 249 (1–2) (2005) 245–249.

- [6] L.M. Robeson, H.H. Hwu, J.E. McGrath, Upper bound relationship for proton exchange membranes: empirical relationship and relevance of phase separated blends, J. Membr. Sci. 302 (1–2) (2007) 70–77.
- [7] H.B. Park, J. Kamcev, L.M. Robeson, M. Elimelech, B.D. Freeman, Maximizing the right stuff: the trade-off between membrane permeability and selectivity, Science 356 (6343) (2017) eaab0530.
- [8] J.W. Barnett, C.R. Bilchak, Y. Wang, B.C. Benicewicz, L.A. Murdock, T. Bereau, S. K. Kumar, Designing exceptional gas-separation polymer membranes using machine learning, Sci. Adv. 6 (20) (2020) eaaz4301.
- [9] J. Wang, K. Tian, D. Li, M. Chen, X. Feng, Y. Zhang, Y. Wang, B. Van der Bruggen, Machine learning in gas separation membrane developing: ready for prime time, Separ. Purif. Technol. 313 (2023) 123493.
- [10] M.L. Cecopieri-Gómez, J. Palacios-Alquisira, J. Dominguez, On the limits of gas separation in CO2/CH4, N2/CH4 and CO2/N2 binary mixtures using polyimide membranes, J. Membr. Sci. 293 (1–2) (2007) 53–65.
- [11] L.M. Robeson, Z.P. Smith, B.D. Freeman, D.R. Paul, Contributions of diffusion and solubility selectivity to the upper bound analysis for glassy gas separation membranes, J. Membr. Sci. 453 (2014) 71–83.
- [12] B.D. Freeman, Basis of permeability/selectivity tradeoff relations in polymeric gas separation membranes, Macromolecules 32 (2) (1999) 375–380.
- [13] L.M. Robeson, M.E. Dose, B.D. Freeman, D.R. Paul, Analysis of the transport properties of thermally rearranged (TR) polymers and polymers of intrinsic microporosity (PIM) relative to upper bound performance, J. Membr. Sci. 525 (2017) 18–24.
- [14] Q. Xu, J. Gao, F. Feng, T.-S. Chung, J. Jiang, Synergizing machine learning, molecular simulation and experiment to develop polymer membranes for solvent recovery, J. Membr. Sci. 678 (2023) 121678.
- [15] G. Ignacz, N. Alqadhi, G. Szekely, Explainable machine learning for unraveling solvent effects in polyimide organic solvent nanofiltration membranes, Adv. Membr. 3 (2023) 100061.
- [16] R. Goebel, M. Skiborowski, Machine-based learning of predictive models in organic solvent nanofiltration: pure and mixed solvent flux, Separ. Purif. Technol. 237 (2020) 116363.
- [17] M. Wang, G.M. Shi, D. Zhao, X. Liu, J. Jiang, Machine learning-assisted design of thin-film composite membranes for solvent recovery, Environ. Sci. Technol. 57 (42) (2023) 15914–15924.
- [18] R. Goebel, T. Glaser, M. Skiborowski, Machine-based learning of predictive models in organic solvent nanofiltration: solute rejection in pure and mixed solvents, Separ. Purif. Technol. 248 (2020) 117046.
- [19] G. Genduso, I. Pinnau, Quantification of sorption, diffusion, and plasticization properties of cellulose triacetate films under mixed-gas CO2/CH4 environment, J. Membr. Sci. 610 (2020) 118269.
- [20] K.P. Bye, V. Loianno, T.N. Pham, R. Liu, J.S. Riffle, M. Galizia, Pure and mixed fluid sorption and transport in celazole® polybenzimidazole: effect of plasticization, J. Membr. Sci. 580 (2019) 235–247.
- [21] Y.J. Lee, R.P. Lively, A transition in diffusion behaviors of organic liquid mixtures in dense polymer membranes, J. Membr. Sci. 713 (2025) 123346.
- [22] R. Mathias, D.J. Weber, K.A. Thompson, B.D. Marshall, M. Finn, J.K. Scott, R. P. Lively, Framework for predicting the fractionation of complex liquid feeds via polymer membranes, J. Membr. Sci. 640 (2021) 119767.
- [23] Y.J. Lee, L. Chen, J. Nistane, H.Y. Jang, D.J. Weber, J.K. Scott, N.D. Rangnekar, B. D. Marshall, W. Li, J. Johnson, Data-driven predictions of complex organic mixture permeation in polymer membranes, Nat. Commun. 14 (1) (2023) 4931.
- [24] G. Zhu, C. Kim, A. Chandrasekarn, J.D. Everett, R. Ramprasad, R.P. Lively, Polymer genome–based prediction of gas permeabilities in polymers, J. Polym. Eng. 40 (6) (2020) 451–457
- [25] W. Lau, A. Ismail, N. Misdan, M. Kassim, A recent progress in thin film composite membrane: a review, Desalination 287 (2012) 190–199.
- [26] A. Ismail, M. Padaki, N. Hilal, T. Matsuura, W. Lau, Thin film composite membrane—Recent development and future potential, Desalination 356 (2015) 140–148
- [27] T. Zhu, Q. Xia, J. Zuo, S. Liu, X. Yu, Y. Wang, Recent advances of thin film composite membranes for pervaporation applications: a comprehensive review, Adv. Membr. 1 (2021) 100008.
- [28] K.A. Thompson, R. Mathias, D. Kim, J. Kim, N. Rangnekar, J. Johnson, S.J. Hoy, I. Bechis, A. Tarzia, K.E. Jelfs, N-Aryl-linked spirocyclic polymers for membrane separations of complex hydrocarbon mixtures, Science 369 (6501) (2020) 310–315.
- [29] N.C. Bruno, R. Mathias, Y.J. Lee, G. Zhu, Y.-H. Ahn, N.D. Rangnekar, J. Johnson, S. Hoy, I. Bechis, A. Tarzia, Solution-processable polytriazoles from spirocyclic monomers for membrane-based hydrocarbon separations, Nat. Mater. 22 (12) (2023) 1540–1547.
- [30] D.W. McCall, D.C. Douglass, Diffusion in binary solutions, J. Phys. Chem. 71 (4) (1967) 987–997.
- [31] R. Krishna, Multicomponent surface diffusion of adsorbed species: a description based on the generalized Maxwell—Stefan equations, Chem. Eng. Sci. 45 (7) (1990) 1779–1791.
- [32] A. Vignes, Diffusion in binary solutions. Variation of diffusion coefficient with composition, Ind. Eng. Chem. Fundam. 5 (2) (1966) 189–199.

- [33] B.D. Marshall, J.R. Johnson, Y.J. Lee, D. Moser, R.P. Lively, Organic solvent reverse osmosis separations of hydrocarbon-alcohol mixtures using matrimid membranes, J. Membr. Sci. 689 (2024) 122168, https://doi.org/10.1016/j. memsci.2023.122168.
- [34] J. Nistane, R. Datta, Y.J. Lee, H. Sahu, S.S. Jang, R. Lively, R. Ramprasad, Polymer design for solvent separations by integrating simulations, experiments and known physics via machine learning, npj Comput. Mater. 11 (1) (2025) 187.
- [35] A. Chandrasekaran, C. Kim, S. Venkatram, R. Ramprasad, A deep learning solvent-selection paradigm powered by a massive solvent/nonsolvent database for polymers, Macromolecules 53 (12) (2020) 4764–4769.
- [36] S.T. Kao, F.J. Wang, S.J. Lue, Sorption, diffusion, and pervaporation of benzene/ cyclohexane mixtures on silver-nafion membranes, Desalination 149 (1) (2002) 35–40, https://doi.org/10.1016/S0011-9164(02)00688-4.
- [37] M. Bahmanyar, S. Sedaghat, A. Ramazani S.A, H. Baniasadi, Preparation of ethylene vinyl acetate copolymer/graphene oxide nanocomposite films via solution casting method and determination of the mechanical properties, Polym.-Plast. Technol. Eng. 54 (2) (2015) 218–222, https://doi.org/10.1080/ 03602559 2014 958772
- [38] A. Khazaei, V. Mohebbi, R.M. Behbahani, A. Ramazani S.A, Pervaporation of toluene and iso-octane through poly(vinyl alcohol)/graphene oxide nanoplate mixed matrix membranes: comparison of crosslinked and noncrosslinked membranes, J. Appl. Polym. Sci. 135 (7) (2018) 45853, https://doi.org/10.1002/ app.45853.
- [39] G. Kung, L.Y. Jiang, Y. Wang, T.-S. Chung, Asymmetric hollow fibers by polyimide and polybenzimidazole blends for toluene/iso-octane separation, J. Membr. Sci. 360 (1) (2010) 303–314, https://doi.org/10.1016/j.memsci.2010.05.030.
- [40] A. Khazaei, V. Mohebbi, R.M. Behbahani, S.A. Ahmad Ramazani, Energy consumption in pervaporation, conventional and hybrid processes to separate toluene and i-octane, Chem. Eng. Process. Process Intensif. 128 (2018) 46–52, https://doi.org/10.1016/j.cep.2018.04.009.
- [41] W. Xu, D.R. Paul, W.J. Koros, Carboxylic acid containing polyimides for pervaporation separations of toluene/iso-octane mixtures, J. Membr. Sci. 219 (1) (2003) 89–102, https://doi.org/10.1016/S0376-7388(03)00188-1.
- [42] H. Wang, J. Li, Microporous metal-organic frameworks for adsorptive separation of C5–C6 alkane isomers, Acc. Chem. Res. 52 (7) (2019) 1968–1978, https://doi. org/10.1021/acs.accounts.8b00658.
- [43] J.F. Denayer, G.V. Baron, J.A. Martens, P.A. Jacobs, Chromatographic study of adsorption of n-Alkanes on zeolites at high temperatures, J. Phys. Chem. B 102 (17) (1998) 3077–3081. https://doi.org/10.1021/ip972328t.
- [44] J.F.M. Denayer, S. van der Beken, K.M.A. De Meyer, J.A. Martens, G.V. Baron, Chromatographic liquid phase separation of n-alkane mixtures using zeolites, in: E. van Steen, M. Claeys, L.H. Callanan (Eds.), Stud. Surf. Sci. Catal. (2004) 1944–1949, https://doi.org/10.1016/S0167-2991(04)80731-6. Elsevier.
- [45] B. Bozbiyik, J. Lannoeye, D.E. De Vos, G.V. Baron, J.F.M. Denayer, Shape selective properties of the Al-fumarate metal–organic framework in the adsorption and separation of n-alkanes, iso-alkanes, cyclo-alkanes and aromatic hydrocarbons, Phys. Chem. Chem. Phys. 18 (4) (2016) 3294–3301, https://doi.org/10.1039/ C5CP06342F.
- [46] H.Y. Jang, J. Johnson, Y. Ma, R. Mathias, D.A. Bhandari, R.P. Lively, Torlon® hollow fiber membranes for organic solvent reverse osmosis separation of complex aromatic hydrocarbon mixtures, AIChE J. 65 (12) (2019) e16757.
- [47] K.A. Thompson, R. Mathias, R.P. Lively, M. Finn, Structure–function relationships in membrane-based hydrocarbon separations using N-aryl-linked spirocyclic polymers, Chem. Mater. 35 (9) (2023) 3464–3469.
- [48] Y. Ren, H. Ma, J. Kim, M. Al Otmi, P. Lin, C. Dai, Y.J. Lee, Z. Zhai, W.J. Jang, S. Yang, Fluorine-rich poly (arylene amine) membranes for the separation of liquid aliphatic compounds, Science 387 (6730) (2025) 208–214.
- [49] I. Pinnau, W.J. Koros, Relationship between substructure resistance and gas separation properties of defect-free integrally skinned asymmetric membranes, Ind. Eng. Chem. Res. 30 (8) (1991) 1837–1840.
- [50] R.Y. Huang, X. Feng, Resistance model approach to asymmetric polyetherimide membranes for pervaporation of isopropanol/water mixtures, J. Membr. Sci. 84 (1–2) (1993) 15–27.
- [51] J.M. Henis, M.K. Tripodi, Composite hollow fiber membranes for gas separation: the resistance model approach, J. Membr. Sci. 8 (3) (1981) 233–246.
- [52] S. Karode, S. Kulkarni, Analysis of transport through thin film composite membranes using an improved Wheatstone bridge resistance model, J. Membr. Sci. 127 (2) (1997) 131–140.
- [53] W. Yan, Z. Wang, J. Wu, S. Zhao, J. Wang, S. Wang, Enhancing the flux of brackish water TFC RO membrane by improving support surface porosity via a secondary pore-forming method, J. Membr. Sci. 498 (2016) 227–241, https://doi.org/ 10.1016/j.memsci.2015.10.029.
- [54] L.E. Peng, Z. Yang, L. Long, S. Zhou, H. Guo, C.Y. Tang, A critical review on porous substrates of TFC polyamide membranes: mechanisms, membrane performances, and future perspectives, J. Membr. Sci. 641 (2022) 119871, https://doi.org/ 10.1016/j.memsci.2021.119871.
- [55] R. Wang, T.-S. Chung, Determination of pore sizes and surface porosity and the effect of shear stress within a spinneret on asymmetric hollow fiber membranes, J. Membr. Sci. 188 (1) (2001) 29–37.